Ad Hoc Networks 166 (2025) 103691

Contents lists available at ScienceDirect

Ad Hoc Networks

journal homepage: www.elsevier.com/locate/adhoc

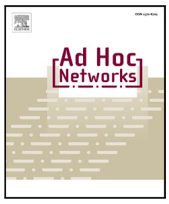

Indoor localization algorithms based on Angle of Arrival with a benchmark comparison

Francesco Furfari, Michele Girolami *, Fabio Mavilia, Paolo Barsocchi

Information Sciences and Technologies Institute ISTI CNR, Via G. Moruzzi 1, 56124, Pisa, Italy

ARTICLE INFO

Keywords:
Indoor localization
Angle of Arrival (AoA)
Bluetooth 5.1 Direction Finding
Outlier filtering

ABSTRACT

Indoor localization is crucial for developing intelligent environments capable of understanding user contexts and adapting to environmental changes. Bluetooth 5.1 Direction Finding is a recent specification that leverages the angle of departure (AoD) and angle of arrival (AoA) of radio signals to locate objects or people indoors. This paper presents a set of algorithms that estimate user positions using AoA values and the concept of the Confidence Region (CR), which defines the expected position uncertainty and helps to remove outlier measurements, thereby improving performance compared to traditional triangulation algorithms. We validate the algorithms with a publicly available dataset, and analyze the impact of body orientation relative to receiving units. The experimental results highlight the limitations and potential of the proposed solutions. From our experiments, we observe that the Conditional All-in algorithm presented in this work, achieves the best performance across all configuration settings in both line-of-sight and non-line-of-sight conditions.

1. Introduction

The past decade, indoor localization techniques have significantly improved in terms of accuracy and availability, driven by the growing demand for location-based services in various IoT scenarios [1,2]. This technological evolution has been marked by the adoption of RF-based technologies, as outlined in [3], and the incorporation of different techniques such as RSS (Received Signal Strength), AoA or AoD (Angle of Arrival and Departure) [4], PDoA (Phase Difference of Arrival), and ToF (Time of Flight). Notably, short-range wireless technologies like Bluetooth [5,6], WiFi, and Ultra Wide Band (UWB) have played a pivotal role in this context.

In 2019, the Bluetooth Special Interest Group (SIG) introduced a new protocol specification as an extension to Bluetooth Core Specification 5.1, known as Bluetooth 5.1 Direction Finding (DF) [7]. Such specification relies on AoD and AoA techniques and is specifically tailored for indoor positioning of objects and people [8,9]. In this setup, the receiving device, such as an anchor deployed within an indoor environment, is typically equipped with an antenna array and a microcontroller responsible for measuring the phase difference of messages transmitted by a tag, as detailed in [10]. The antenna can estimate the AoA on two planes: azimuth and elevation thus enabling the position estimation of a moving target.

In this study, we present a set of increasingly complex algorithms for indoor positioning based on Angle of Arrival (AoA) estimation. The proposed algorithms are based on the concept of Confidence Region (CR) useful to estimate the actual target's location. More specifically, given a set of anchor nodes estimating azimuth angles for a given target, the CR is defined as the region of uncertainty regarding the actual position of the target. The CR can be determined through a geometric process and subsequently such region can be used to validate the position of the target. Given a CR, position estimates made by each anchor that do not belong to the region are potential outliers and are excluded from the position estimation process. In fact, in real-world scenarios, several factors can impact the reliability of measurements. Multipath effects and reflections can introduce delays and distortions in received signals. Measurements that are unreliable due to these factors are often referred to as anomalies in machine learning and outliers in statistics [11,12]. Classical methods can be so heavily influenced by outliers that the resulting model may be entirely inaccurate. One approach to addressing the outlier problem is to identify and remove them. The issue of outliers is increasingly becoming a significant research focus, with various terms used in the literature, such as robust methods, anchor selection, and outlier filtering.

We introduce the *All-in Region*, *All-in Circle*, and *Conditional All-in Circle* algorithms, and we compare their performance against various baseline methods. Rather than starting with the traditional linear least squares solution (LLS) – which provides a suboptimal result that can be

* Corresponding author.
E-mail addresses: francesco.furfari@isti.cnr.it (F. Furfari), michele.girolami@isti.cnr.it (M. Girolami), fabio.mavilia@isti.cnr.it (F. Mavilia), paolo.barsocchi@isti.cnr.it (P. Barsocchi).

https://doi.org/10.1016/j.adhoc.2024.103691
Received 24 June 2024; Received in revised form 16 September 2024; Accepted 18 October 2024
Available online 25 October 2024

improved through a weighted solution (WLLS) when angular measurement statistics are available – we opted for a minimal solution. This approach calculates the centroid of all possible intersections from the angular directions, while excluding potential outliers.

This method is particularly suited for mobility scenarios where it is difficult to collect statistics on the reliability of angular measurements, making it challenging to apply methods like WLLS or more accurate, yet computationally intensive, non-linear methods such as Maximum Likelihood (ML). Despite this, the results show that the proposed methods can achieve even better outcomes than traditional approaches.

Our performance assessment is based on the analysis of a real-world dataset, as reported in [13], which is publicly available.[1] The selected dataset provides Angle of Arrival (AoA) measurements from four anchor nodes positioned across a wide indoor area. Data were collected under three distinct application scenarios: static target, where the target remains stationary in the same position for a specified period; moving target, where the target moves throughout the room; and proximity, where some targets move in close proximity to each other. Each dataset is annotated with ground truth information, which is the actual position of the target, to validate performance. Based on our experiments, the Conditional All-in algorithm demonstrates the best performance, with the 90th percentile of the localization error being less than 2.00 m, the 75th percentile below 1.50 m and the 50th percentile below 1.00 m.

The contribution of the proposed work can be summarized as:

- the introduction of a geometrical process bounding the target's position. This process can be adopted in both AoA-based and AoD-based algorithms;
- the definition of three algorithms of increasing performance and decreasing computational complexity, enabling the estimation of a static/moving target indoor;
- the performance evaluation of the algorithms using real data collected from Bluetooth 5.1-compliant hardware. The dataset, along with ground truth annotations, is made available to the community for the sake of repeatability;

The remind of this paper is organized as follows. In Section 2 we introduce the basic elements of the Direction Finding specification and triangulation techniques. In Section 3 we survey existing works based on AoA for indoor localization, Section 4 we introduces the CR-based algorithms. The performance evaluation is reported in Section 5, while Section 6 discusses the use of AoA for indoor localization.

Furthermore, for better understanding, we provide a table in Appendix, explaining all the abbreviations used in the paper.

2. Background knowledge

We first introduce the Bluetooth 5.1 Direction Finding (DF) specification, and then some concepts of triangulation techniques based on the estimation of directions.

2.1. The Direction Finding specification

To accurately determine the AoA of signals transmitted by a mobile target, it is crucial to equip receivers with an antenna array [10]. The antenna array typically consists of multiple antenna elements arranged in a specific geometric pattern, such as a uniform linear array (ULA) or a uniform rectangular array (URA). AoA is derived through the measurement of phase difference γ within signals captured by adjacent antennas, employing RF radiogoniometry techniques. This calculation leverages the knowledge of the signal's wavelength λ and the antenna geometry, which includes the distance d between the antennas.

[1] https://doi.org/10.5281/zenodo.7759557

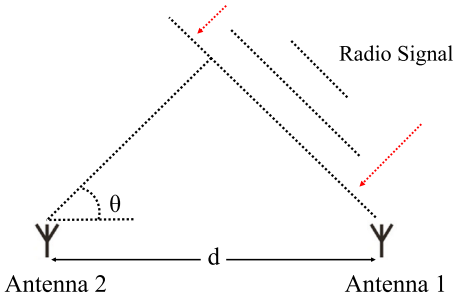

Fig. 1. AoA computation based on the geometry of the antenna array.

As reported in Fig. 1, assuming the radio signal is a plane wave with a constant frequency impinging on the antenna array of the receiver, AoA θ can be easily calculated by the formula $\theta = \arccos(\frac{\lambda\gamma}{2\pi d})$. The formula represents a basic model for AoA calculation. More complex algorithms are often employed to account for various factors such as multipath propagation, antenna mutual coupling, and noise. These advanced techniques may include MUSIC (Multiple Signal Classification), ESPRIT (Estimation of Signal Parameters via Rotational Invariance Techniques), or machine learning-based approaches.

The Bluetooth 5.1 specification enables the determination of AoA by introducing a Constant Tone Extension (CTE) to the Protocol Data Unit (PDU) format of BLE messages. The CTE is a crucial component of the DF feature, as it provides a stable signal for accurate phase measurements. The CTE follows the CRC code, as shown in Fig. 2 and consists of a sequence of unwhitened 1-valued bits with variable length between [16–160] μs; this extension guarantees a constant frequency for this part of the Bluetooth signal. Throughout the CTE period, the anchor equipped with an antenna array can obtain In-Phase and Quadrature (IQ) samples without the influences of modulation. Finally, given the IQ samples the anchor effortlessly estimates the information about the received signals, such as the phase difference from which computing the AoA on the azimuth and elevation. The ability to determine both azimuth and elevation angles represents a significant advancement in indoor positioning technology, enabling new applications and improved accuracy of three-dimensional positioning systems for location-based services.

2.2. AoA-based techniques

The DF specification standardizes angle estimation, and commercial products are increasingly available that enable position estimation using triangulation or multiangulation techniques.

Differently from RSSI-based trilateration [14], which requires three anchors to estimate the target's position, the AoA-based technique only requires one anchor to estimate the target's planar coordinates, given the target's height h. In particular, the cone generated by the target's elevation angle can be intersected with an orthogonal plane with respect to the azimuth plane, along the azimuth direction (as studied in [15]). However, when the target's height h is unknown, then two anchors are required to estimate the target's position. In this last case, the estimated position can be calculated by intersecting the straight lines representing the azimuth directions.

In this work, we focus on the second case previously mentioned. More specifically, our scenario consists of multiple anchors arranged vertically on the walls of the indoor environment. In this way the azimuthal plane of the anchors is parallel to the walking surface and allows us to simplify the study on the XY plane by excluding information on elevation. The Fig. 3 shows a graphical representation of the indoor environment, where anchors A1 and A2 are deployed on the adjacent walls. The azimuth angle (ϕ) for each anchor ranges from −90° to 90° (left to right in Fig. 3). The target is represented as a red dot,

Preamble (1 or 2 octets)	Access-Address (4 octets)	PDU (2-258 octets)	CRC (3 octets)	Constant Tone Extention (16-160 µs)

Fig. 2. Bluetooth packet format supporting Direction Finding capability.

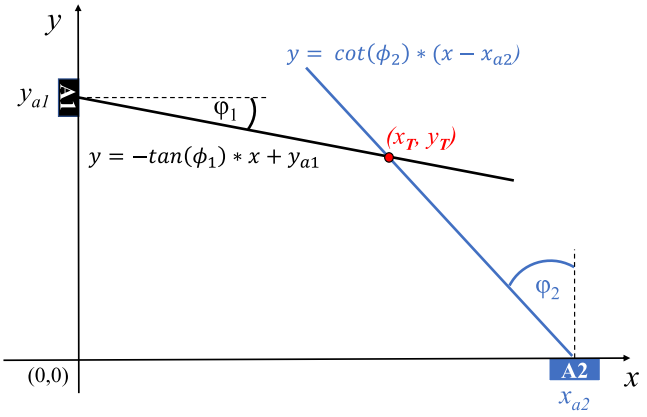

Fig. 3. Position estimation using azimuth angles.

and its location (x_T, y_T) can be estimated with the linear equations of the directions provided by the 2 anchors:

$$(\mathbf{Ax} = \mathbf{b}) \equiv \begin{cases} \tan(\phi_1) \cdot x + y = y_{a1} \\ -\cot(\phi_2) \cdot x + y = -\cot(\phi_2) \cdot x_{a2} \end{cases} \quad (1)$$

whose solution can be obtained with the Cramer's rule, as follows:

$$x_T = \frac{D_x}{D} = \frac{y_{a1} + \cot(\phi_2) \cdot x_{a2}}{\tan(\phi_1) + \cot(\phi_2)}; \quad (2)$$

$$y_T = \frac{D_y}{D} = \frac{\cot(\phi_2) \cdot (y_{a1} - \tan(\phi_1) \cdot x_{a2})}{\tan(\phi_1) + \cot(\phi_2)} \quad (3)$$

However, it is important to remark that the validity of Eq. (1) is restricted to only four *critical conditions*, as detailed in the next.

Parallel and Coincident Lines: the resulting system from Eq. (1) is indeterminate, i.e., when the determinants D, D_x, D_y are 0, then the detected directions by anchors are parallel and coincident, as shown in Fig. 4(a) Such condition happens when the target's location is located anywhere along the connecting line between the anchors A1 and A2.

Parallel lines: the anchor's directions are parallel but not coincident, i.e., when $D = 0$ and $D_x \neq 0$ or $D_y \neq 0$, as depicted in Fig. 4(b). In these cases, Eq. (1) does not admit any valid solution. An alternative approach would be to deploy the third anchor, adding one more equation to the linear system given in Eq. (1).

Outside intersections: there exist a valid intersection between the anchor's directions, i.e., $D \neq 0$, but the estimated location of the target lies outside the environment, as shown in Fig. 4(c). In this case, anchors estimate slightly different directions of the target, and the resulting intersection point falls beyond the boundary of the environment. Nevertheless, this situation can be mitigated by intersecting the lines with the boundaries of the environment.

Amplified error: the target is located along the line connecting the two anchors, but small measurement errors amplify the localization error, projecting the intersection of lines far from the target, as shown by the red square in Fig. 4(d).

When several angular measurements are available, obtained by deploying multiple anchors in the environment, system (1) becomes overdetermined, i.e. the number of equations m is greater than the number of unknowns n.

$$\mathbf{Ax} = \mathbf{b}, \text{ with } \mathbf{A} \in \mathbb{R}^{m,n}, \mathbf{x} \in \mathbb{R}^n, \mathbf{b} \in \mathbb{R}^m \text{ and } m \geq n \quad (4)$$

These systems of equations are solved using the linear least squares (LLS) method. It involves minimizing the distance between the vector **Ax** and the vector **b**, called residual, which is achieved by multiplying the pseudoinverse matrix of **A** by **b**.

$$\hat{\mathbf{x}}_{LLS} = (\mathbf{A}^T\mathbf{A})^{-1}\mathbf{A}^T\mathbf{b} \quad (5)$$

Accuracy of LLS methods can be improved by including a weight matrix **W**. Qualitatively, the matrix introduces the effect of the noise statistics in the estimation of angles and allows to improve the localization algorithm adding information on the reliability of the single equation of the linear system. The weight matrix, each observation being independent, is a diagonal matrix given by:

$$W = \Sigma^{-1} = \text{diag}\left(\frac{1}{\sigma_{\phi_1}^2 d_1^2}, \frac{1}{\sigma_{\phi_2}^2 d_2^2}, \ldots, \frac{1}{\sigma_{\phi_M}^2 d_M^2}\right) \quad (6)$$

where $\sigma_{\phi_i}^2$ is the azimuth variance and d_i the distance from the ith anchor. The problem is that with the angular measurements we cannot also obtain a distance measurement. An efficient way is to proceed in two steps: first we apply Eq. (5) of the LLS method and then with the distance estimate we proceed to calculate the weights and the weighted solution (WLLS) given by equation:

$$\hat{\mathbf{x}}_{WLLS} = (\mathbf{A}^T\mathbf{WA})^{-1}\mathbf{A}^T\mathbf{Wb} \quad (7)$$

The variance requires a certain observation period to be calculated correctly, which implies that the target should remain stationary during the observation window.

3. Related works

In recent years, there has been a growing interest in the development and assessment of various radio frequency (RF) techniques and technologies for indoor positioning [16]. This interest can be attributed to the widespread use of mobile devices that are pervasive, personal and ubiquitous, that are frequently employed for accurate target localization [17,18]. As depicted in Fig. 5, signal metrics are combined with RF technologies and positioning methods in the existing literature. A comprehensive survey of scientific papers was conducted, resulting in the selection of 16,077 relevant articles from the state-of-art digital libraries. These articles specifically concern to RF technologies applied within indoor positioning systems. It is noteworthy that only a small subset of the existing papers, are focused around the Angle of Arrival (AoA) metric for user localization and adopting triangulation techniques.

For instance, in [19], authors examine the precision of AoA localization with just two anchors. This study introduces the concept of the *ambiguity area* for assessing localization precision based on AoA estimation errors at anchor nodes. However, it solely provides mathematical formulations to evaluate the user's precision area without presenting a localization algorithm. In contrast, our research employs four anchors in a real-world setting, introducing a method to further diminish uncertainty areas and enhance traditional triangulation-based algorithms. In [20], an improved pseudolinear estimator (IPLE) using azimuth and elevation angles is proposed. However, the IPLE is not an unbiased estimator. To address this, an improved weighted instrumental variable estimator (IWIV) is developed. In [21], authors derive pseudolinear equations and apply the weighted least-squares (WLS) technique and a bias-reduced solution based on WLS (WLS-BR). Nonetheless, these solutions are computationally intensive. Therefore, [22] introduces an iterative AoA localization method to reduce complexity. Such work emphasizes convergence and performance in simulation scenarios, but

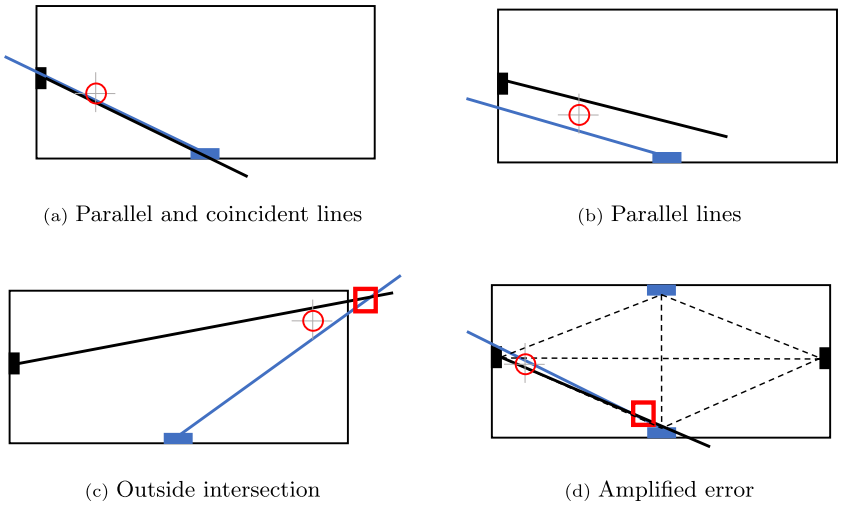

(a) Parallel and coincident lines (b) Parallel lines

(c) Outside intersection (d) Amplified error

Fig. 4. Limits of the AoA-based localization: we report 4 critical conditions.

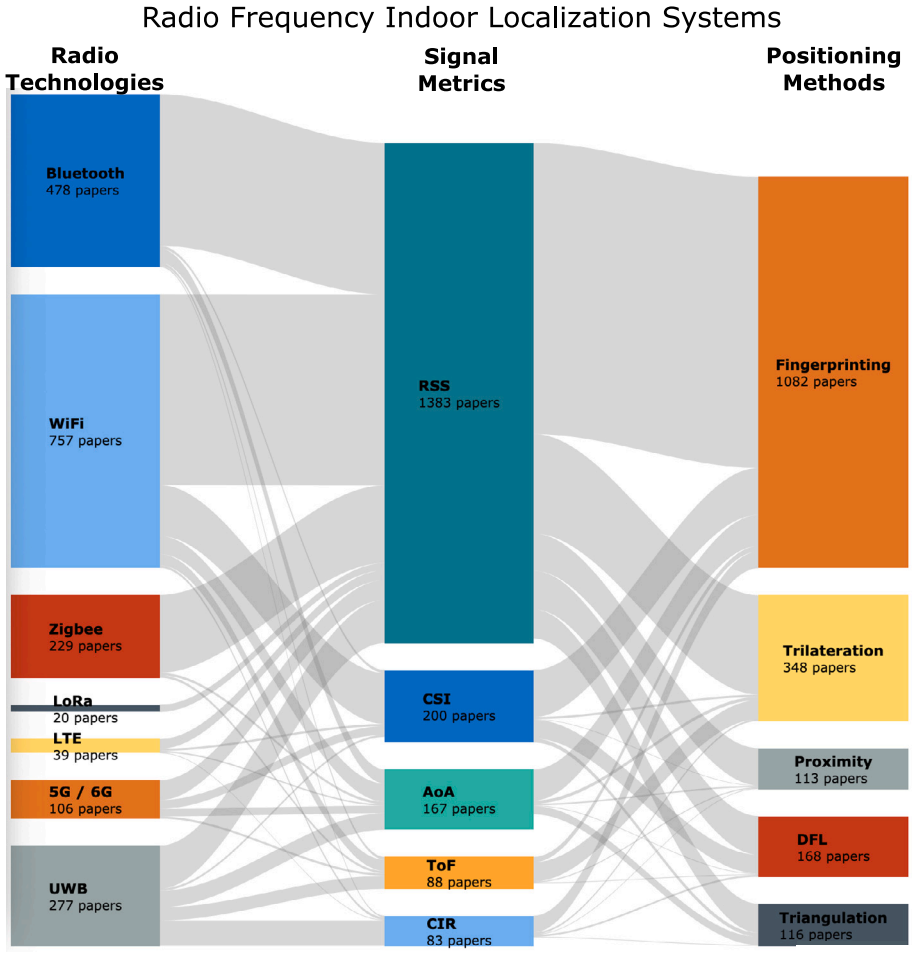

Fig. 5. Alluvial diagram showing the relationship between Radio Technologies, Signal Metrics and Positioning Methods (DFL stands for Device-Free Localization). Data are extracted from Scopus digital library.

lacks experimental validation with real-world data or practical implementation, limiting its real-world applicability. Lastly, in [23,24], authors propose an eigenspace solution for source localization using modified polar representation (MPR).

While the aforementioned studies are primarily theoretical or simulation-based, only few works assess localization algorithms through real-world experiments. In [25], authors introduce a scenario featuring two fixed receiver anchors using Software Defined Radios (SDR) to replicate Constant Tone Extension (CTE) packets. They achieve an average positioning error of approximately 85 cm across 20 locations. In [10], an innovative hybrid approach combines both Angle of Arrival (AoA) and Received Signal Strength Indicator (RSSI)

data from Bluetooth signals to estimate the transmitter's location. This experiment is conducted in a real 25 × 15 m laboratory environment with four receiving anchors, resulting in an average sub-meter error of about 70 cm, calculated from just eight locations using a barycenter method. Additionally, in [26], position error estimates are made in both indoor and outdoor settings. In indoor tests, two anchors are placed in a small 5 × 5 m room with 2-m spaced locations. The study achieves a mean error of approximately 36.5 cm across just four locations. In [27], authors evaluate outdoor localization error performance, reporting a localization error of 22 cm, although only at one specific position. This single point of data is insufficient to draw generalized conclusions for indoor environments. Lastly, authors in [28] assess positioning error with the barycenter method within a smaller 4.8 × 4.8 m area, yielding a 70 cm error, though it does not account for the user's posture in a static scenario.

More recent works address the adoption of AoA-based technique combined with outlier filtering, anomaly detection and anchor selection strategies with the goal of optimizing the position estimation. Authors of [29] evaluates AoA estimation accuracy in multipath environments and proposes a weighted AoA-based localization method. An approximate method for assessing AoA accuracy is developed due to practical limitations in available receiver information. Simulations show that the proposed weighted approach reduces median localization error by 20% compared to unweighted methods. In [30] authors present an RSSI-based indoor localization system using Wi-Fi infrastructure and introduces a new continuous-feature-scaling model for the k-nearest neighbor algorithm. The gridless scheme eliminates the need for dividing RSSI space into intervals, improving accuracy and avoiding issues with weight selection at boundaries. Experimental results demonstrate the method's superior performance, achieving localization errors of 1.34 m and 1.72 m in different indoor environments. Still based on outlier detection, the work presented in [31] addresses the nonlinear challenges in indoor position estimation using Angle of Arrival (AoA) measurements. The paper analyzes the impact of deployment geometry through analytical methods and Monte-Carlo simulations. To overcome limitations in single and multi-anchor setups, a multi-anchor solution with outlier rejection is proposed, accounting for the model's nonlinearity. The method approximates the node's position probability distribution using an unscented transformation of AoA estimates, with a majority voting scheme to eliminate outliers. Bayesian inference is then applied to fuse the data, and real-world tests using Bluetooth demonstrate the approach's practicality, robustness, and accuracy.

In [32] authors presents a real-time indoor localization system using commodity WiFi infrastructure, addressing the unresolved challenge of accurate localization. The system introduces a non-parametric metric for AoA accuracy, a co-localization algorithm leveraging relationships among multiple APs, and strategies to reduce computational complexity. Experiments demonstrate the system's superior performance, achieving a 4-degree median AoA estimation error and 30 cm localization median error. In [33] authors adopt an outlier filtering approach. In particular, the work introduces a novel outlier-robust filter for nonlinear dynamical systems, designed for measurements from independent sensors. The method modifies the measurement model and applies Variational Bayes theory and general Gaussian filtering, selectively rejecting corrupted data. Simulations with varying sensor numbers show that the proposed filter is more computationally efficient than similar methods, while maintaining comparable estimation quality. Real-time indoor localization experiments using UWB sensors confirm the practical effectiveness of the approach. A different approach consists in using the factor graphs as adopted in [34,35]. In [34] authors present a unified framework for high-accuracy indoor localization, integrating ranging and fingerprinting techniques for the Internet of Things (IoT) applications. The framework uses a non-parametric belief propagation algorithm to achieve accurate position estimation with moderate computational complexity, while minimizing crowdsourcing efforts for fingerprinting databases. A likelihood-ratio-based method enhances robustness by detecting ranging outliers, and a low-complexity serial scheduling scheme enables real-time localization. Experimental results using a hybrid ultrawide bandwidth and Wi-Fi system show the proposed method achieves submeter accuracy. In [35] authors present a tightly coupled fusion platform for indoor smartphone localization, integrating Wi-Fi RTT, RSS, and data-driven pedestrian dead reckoning (DPDR) using factor graph optimization (FGO). The proposed system, incorporating magnetic information (MI), tracks pedestrians at 20 Hz while supporting various smartphone usage poses. Experimental comparisons show that the platform achieves an average positioning accuracy of 0.39 m, improving the accuracy of extended and adaptive robust Kalman filters by 45.83% and 27.78%, respectively.

Compared to existing state-of-the-art approaches, the algorithms introduced in this paper are assessed within a more realistic scenario for two main reasons:

- we adopt realistic and open data collected with an accurate data collection campaign [13];
- we test our algorithms by considering the impact of human body to the resulting performance.

Emphasizing the importance of reproducibility in our evaluation we draw from [36,37] as valuable guidelines to design a consistent, accurate, and robust data collection process.

4. Indoor localization through confidence regions

4.1. Confidence regions

In this section, we introduce the concept of *Confidence Region*, a topological region exploitable to improve the accuracy of a set of indoor localization algorithms.

Given a pair of anchors, namely A1 and A2, and a target T in the environment, since the random variables associated with the error in the AoA measurement are independent and of the same type, the joint Confidence Region (CR) can be obtained as the Cartesian product of the confidence intervals of each variable. In a graphical representation, boundary directions can be associated with the bounds of the confidence interval of each variable or anchor. By intersecting the boundary directions for each anchor a polygon is obtained whose area represents the uncertainty of the joint measurement. We show in Fig. 6 a graphical represented of CRs for two targets: T_1 and T_2. In the figure, CRs are represented as red-closed polygons resulting from the intersection of the dotted lines. The existence of a CR gives rise to the possibility of restricting the target's position. In particular, we observe that given a CR, the max uncertainty for a given target is always bound by the corresponding CR's width.

The example reported in Fig. 6 shows two interesting situations in which targets T_1 and T_2 are at different distance from anchors A_1 and A_2. In the case of T_1, its CR's area is smaller then the T_2, as the area of a confidence region depends on how close the target is with respect to anchors. As a result, the localization error of for T_1 is always lower than that of T_2.

4.2. Indoor localization algorithms

We now introduce three algorithms exploiting the geometrical properties of the confidence regions and designed to reduce the localization error, namely *All-in Region*, *All-in Circle* and *Conditional All-in Circle*.

The target position can be estimated according to equations reported in Section 2.2. More specifically, a basic approach consists of computing the geometric barycenter (or centroid), of the intersections obtained from the linear system reported Eq. (1). The result of such system returns a set of intersection points, i.e. given 4 anchors $A_1 \cdots A_4$, the system in Eq. (1) results with 6 points: anchor A_1 intersects with

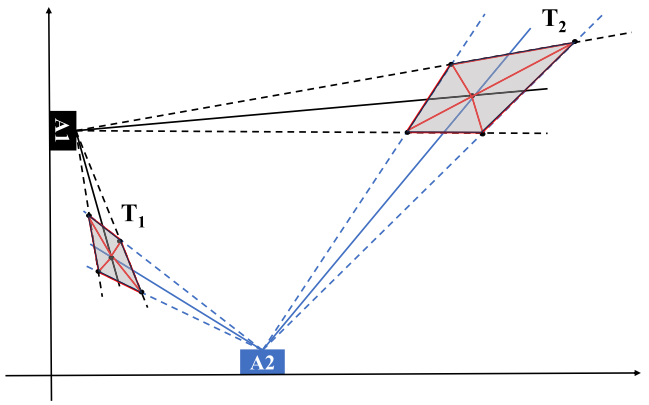

Fig. 6. Red polygons show a graphical representation of the Confidence Region obtained by intersecting anchor's boundary directions.

A_2, A_3, A_4, anchor A_2 intersects with A_3, A_4 and anchor A_3 intersects with A_4.

However, we observe that exploiting *all* the intersections is not always advantageous, as shown with the critical conditions reported Figs. 4(c) and 4(d). In these two cases, the error in specific areas is amplified, altering the computation of the centroid used as approximation of the target's position. A possible solution, is to exclude from the estimation of the target's position, those intersection points falling outside the environment. Nevertheless, such filtering does not completely remove any possible error, even large ones, that can project the anchor's intersections far from the actual target's location.

The first algorithm we propose is named *All-in Region* and it is described in Algorithm 1. Given $n > 1$ the number of anchors, we define I the set of intersection points of n anchors, where $|I| = T_n = n{\cdot}(n{-}1)/2$, and ϵ is the mean AoA-error expressed in degrees on the azimuth estimated by anchors.

Algorithm 1: All-in Region

Data: $I = \{\ p_i |\ \ p_i \in \mathbb{R}^2,\ \ 0 < i \leq T_n\}$
Result: $b \in \mathbb{R}^2$
b = compute barycenter $< I >$
$polygon$ = compute CR $< \epsilon, b >$
if $(|I| > s \wedge (\exists p \in I \ \ |p \notin polygon))$ **then**
  $\overline{p} = p_i \ | \ max_i(\|b - p_i\|)$;
  return All-in Region $< (I - \{\overline{p}\}) >$;
else
  return(b);
end

The algorithm originates from following observation: it tries to exclude those intersection points that strongly alter the centroid used to estimate the target's location. The proposed algorithm relies on the concept of Confidence Region previously introduced: if the position measurement is accurate, then all the intersection points that contribute to compute the centroid should lie within the CR associated with the centroid. Therefore, the first step of *All-in Region* is to compute the resulting centroid and then the CR. Then the algorithm checks that all the intersection points fall within the CR. If they are all included, then it means that measurements provided by anchors are accurate and deviated from the true position of the estimated mean error. In this case, the algorithm terminates returning the centroid as the estimated target's position. Differently, in case some of the points fall outside the CR, then the algorithm may choose excluding the one that is farthest from the centroid position and recursively, it repeats this procedure with the remaining set of intersection points. At this point, a new centroid and the corresponding CR is re-calculated. The recursion stops with two conditions:

- when either all the intersection points fall within the CR region;
- if only one intersection point exists.

Indeed, even a single intersection point can be considered as a valid estimation of the target's position, since it is calculated from the azimuth directions of two anchors, which is the minimum requirement for estimating a position. We show in Fig. 7 the iterative process of *All-in Region* to estimate the target's position, based on real data available in the dataset [13]. The actual target's position is (840, 240). Iteration *a* in Fig. 7 shows the ground truth as a red point and the confidence region as red polygon obtained by using 6 intersection points. The estimated position is shown as a pink-colored point, corresponding to the centroid of the confidence region. As a result after the first iteration, the estimated position is 88 cm away from the actual position. During iteration *b*, *All-in Region* drops the intersection point labeled 13, originating from the intersection of directions from anchors 1 and 3. A new centroid is computed with the corresponding confidence region, and the obtained error decreases to 63 cm. However, there are still intersection points falling outside the confidence region. Therefore, the algorithm iterates again by excluding intersection point 14. The new confidence region and its centroid, which is now 64 cm away from the ground truth (iteration *c*). Finally, the algorithm iterates again by excluding intersection point 12 as reported with iteration *d* which represents the final iteration of the algorithm. In this last case, all the remaining intersection points fall within the confidence region associated with the centroid, which is now 35 cm away from the ground truth.

The computational cost of *All-in Region* is mainly determined by the operations of intersecting polygons to determine the confidence region, and by verifying whether an intersection point belongs to a confidence region. Various computer graphics algorithms can be used, such as the Weiler–Atherton clipping algorithm [38] and the winding number algorithm, which have complexities of $O(n \cdot log(n))$ and $O(log(n))$, respectively. In our case, the number of sides or vertices (n) will never be too high, and the cost is generally low. However, the challenge of reducing computational costs remains, as position estimation in AoA-based systems is typically performed on the server side, and the algorithm needs to scale with the number of localizations performed per second. One possible solution is to perform the computational cost offline, meaning that confidence region polygons can be calculated beforehand and stored along with the coordinates of the point on a map. Alternatively, instead of storing the polygon, its maximum amplitude can be recorded, and the polygon can be approximated with a circle.

This last observation leads us to an improved version of *All-in Region* with a lower computational cost. The key-observation is to approximate the shape of the confidence regions with a circle of radius R. The *All-in Circle* algorithm is reported in 2.

Algorithm 2: All-in Circle

Data: $I = \{\ p_i |\ \ p_i \in \mathbb{R}^2,\ \ 0 < i \leq T_n\}$
Result: $b \in \mathbb{R}^2$
b = compute barycenter $< I >$
if $(|I| > s \wedge (\exists p \in I \ \ | \ \ (\|b - p\| > R)))$ **then**
  $\overline{p} = p_i \ | \ max_i(\|b - p_i\|)$;
  return All-in Circle with $< (I - \{\overline{p}\}) >$;
else
  return(b);
end

Finally, we introduce the last algorithm, namely *Conditional All-in Circle*. The key idea is to consider that not all anchors are equally

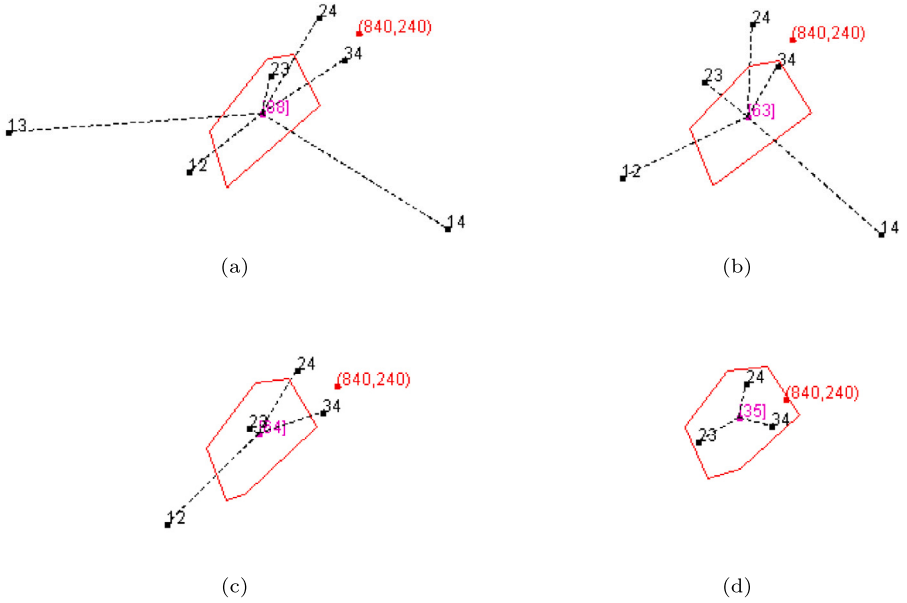

Fig. 7. All-in Region algorithm's steps for estimating position at coordinates (840, 240).

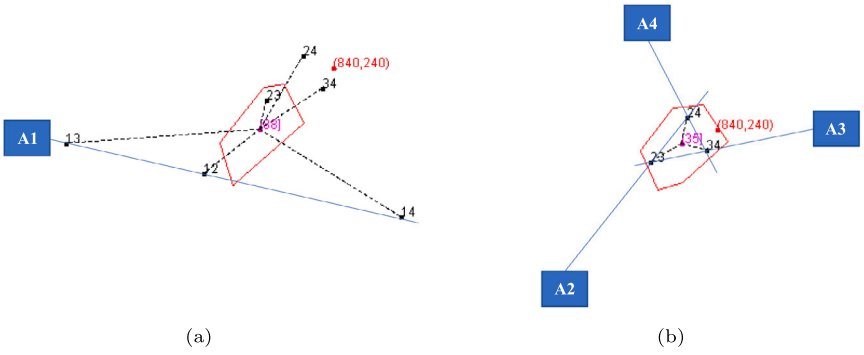

Fig. 8. Direction of the excluded points.

important to build a confidence region. The Conditional All-in Circle algorithm is equal to All-in Circle except from the size of the initial set of intersection points I. One simple rule that can be applied is to dynamically exclude the anchors further from the target. In fact, at the same angle the distant anchors subtend a larger area than that already restricted by anchors closer to the target. More details on how the anchors contribute differently to the determination of the confidence region are provided in Section 5.

In the previous example the target under consideration is located on the right side of a 12 m wide room. The furthest anchor is Anchor 1, which is on the opposite side of the room. Fig. 8 again shows the initial and final stage of the previous iteration process, highlighting the excluded points 12, 13, 14 all belonging to the direction estimated by Anchor 1. Fig. 8 (a) represents the direction estimated by anchor 1. The box on the right highlights the directions of the rest of anchors which are closer to the ground truth. Therefore, if those anchors that are more likely to introduce errors are excluded in advance, the computation is simplified.

5. Experimental settings and results

We will now outline the experiments conducted to assess the effectiveness of the algorithms presented in Section 4.2. Initially, we introduce a simulation tool specifically designed to assess the performance of the algorithms with the related placement of anchors within an indoor setting. This simulation offers an initial insight into anchor positioning, helping us in the selection of an actual dataset. Subsequently, we detail the dataset chosen for our study and present the resultant findings.

5.1. Optimal anchor's layout

The simulation tool allows for the arbitrary placement of anchors and the calculation of resultant confidence regions. To achieve this, the simulator is configured to replicate a 12 × 6 m environment equipped with 4 anchors situated along the perimeter. The simulator implements Eq. (1), one for each of the 4 anchors, yielding 6 distinct linear systems capable of determining 6 points of intersection. The confidence regions are then derived as the intersections of various polygons generated by the linear systems representing boundary directions. The boundary directions depend on the average angular error assumed for the anchors.

The simulator provides a set of metrics useful to evaluate any possible layout. In particular, it provides area of the confidence region, maximum and minimum localization error, and the number of sides of the polygon. Furthermore, when given a set of Angle of Arrival (AoA) measurements, the simulator executes the algorithms outlined in Section 4.2 to estimate the target's position. In Fig. 9 we present 21 distinct confidence regions derived using the method previously described. Anchors are numbered from 1 to 4 and depicted as blue box, and are positioned at the midpoint of the room's walls. The resulting confidence regions exhibit varying shapes of increasing complexity,

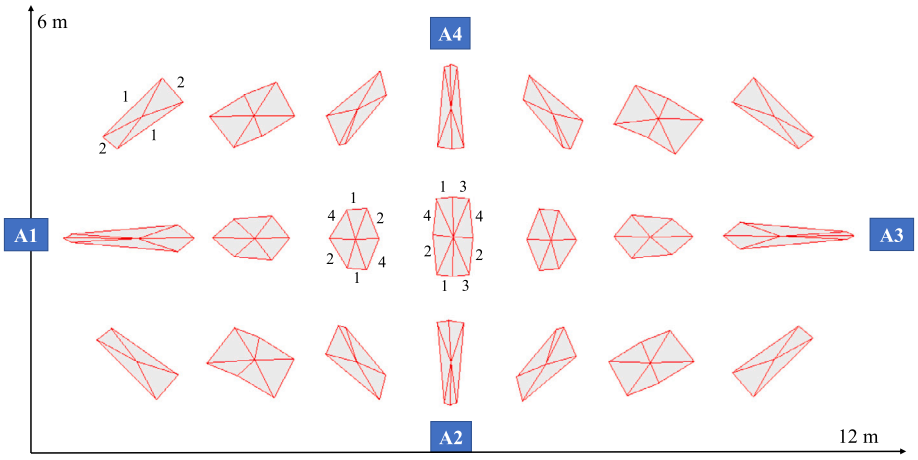

Fig. 9. Confidence regions at different positions of a room obtained with 4 anchors.

Table 1
Simulation results of the localization error obtained with corner or mid layouts.

Az. Err	Mean err.	Min err.	Max err.	Anchor's layout
5°	0.82	0.52	1.28	corner
uniform	**0.59**	**0.40**	**1.08**	**mid**
10°	1.70	1.06	2.51	corner
uniform	**1.20**	**0.85**	**1.95**	**mid**

ranging from triangles to octagons. The centroid of each polygon serves as the target position for which these regions have been computed. The numbers shown on sides of the polygons in Fig. 9 indicate the contributing anchor responsible for defining that particular side of the polygon.

It is noteworthy that in the center of the room, the confidence region adopts an octagonal shape, a result of the combined influence of all four anchors. Conversely, moving to the left, the next region takes on a hexagonal shape, determined by three anchors. Finally, in the upper left corner of Fig. 9, we observe a quadrilateral shape defined by only two anchors. Notably, anchor 3, situated on the right-side wall, becomes less informative for positions exceeding half the room's width. The boundary directions of anchor 3, beyond a distance of 6 m, become too broad to further narrow down the areas derived from the intersections of the other boundary directions. It is important to emphasize that even for the quadrilateral highlighted in the upper left corner, the contribution of anchor 4 is no longer necessary.

Through an analysis of the confidence regions and the average error resulting from placing anchors in different zones within the room, we can assess which configuration is optimal for minimizing position estimation errors. To this end, Fig. 10 illustrates the localization error generated by two anchor layouts: the corner layout and the mid-layout. In both layouts, we assume a uniform azimuth error of 5°. A summary of the performance for these two layouts is provided in Table 1, which includes the calculation of the mean positioning error based on azimuth error and anchor arrangement. From the results, it is clear the theoretical advantage of using the mid-layout, where anchors are deployed on the middle of the walls. Following the results obtained with the simulation process, we selected the mid-layout to deploy anchors in the testing environment.

It is important to note that the results obtained are equivalent to applying geometric dilution of precision (GDOP) procedures [39] to the configurations examined. Specifically, the figures can be derived by calculating the horizontal dilution of precision (HDOP), which focuses on the XY plane and uses the trace of the 2-dimensional Jacobian matrix. However, this evaluation does not account for experimental measurements and environmental factors. For a detailed analysis of the impact of angle estimation errors, please refer to Section 6.1.

5.2. The experimental dataset

We conducted experiments using data collected in a prior study [13]. It is important to note that the dataset is publicly available.[2] The testing environment is a wide indoor room, approximately covering an area of 110 m^2, with no obstructions inside. Four anchor nodes are strategically positioned within the room based on the mid-layout configuration (see Section 5.1). These anchor nodes are mounted on tripod heads at a height of 2.3 m from the ground. The floor is tiled with 60 × 60 cm tiles.

For our hardware setup, we utilized equipment provided by ublox, specifically the XPLR-AOA kit adhering to the Bluetooth 5.1 specification. This kit comprises both anchor nodes and tags. The anchor nodes are compact boards measuring 11.5 × 11.5 cm and are equipped with an array of 5 square-shaped C211 antennas and the NINA-B411 BLE module.[3] These anchor nodes also feature a USB I/O port and are connected to a Raspberry PI board.

As for the tags, they are powered by the NINA-B406 chipset[4] and receive power through a USB port. The tags broadcast BLE beacons at various intervals, including 1, 10, and 50 Hz, and with varying power emissions ranging from −40dBm to 8dBm, as depicted in Fig. 11.

The dataset provides data collected in 4 testing scenario: calibration, static, mobility, and proximity. For the purpose of this work, we analyze data available with the calibration and static scenarios. Concerning the calibration scenario, as reported in Fig. 12, data are collected by employing four anchors and a single tag that is affixed to a tripod and placed in 119 distinct positions within the testing area. This calibration setup is designed to facilitate the examination of how Angle of Arrival (AoA) and Received Signal Strength (RSS) change under *stable* and consistently replicable circumstances. The 119 positions are evenly distributed throughout the entirety of the testing environment. Concerning the static scenario, data are gathered from four anchors and one tag, which is worn by an individual in 36 distinct locations spaced 1.20 m. The 36 positions used in the static scenario are a subset of 119 selected in the calibration scenario and are indicated with the green color in Fig. 12. The tag is attached to a lanyard around the person's neck (1.13 m from the ground). Data collection is performed with the individual facing North, South, East, and West in order to facilitate the examination of how body positioning affects the collected data. The calibration and static scenario provides us about 800.000 samples for each anchor.

[2] https://zenodo.org/record/7759557
[3] https://www.u-blox.com/en/docs/UBX-20035327
[4] https://www.u-blox.com/en/docs/UBX-19049405

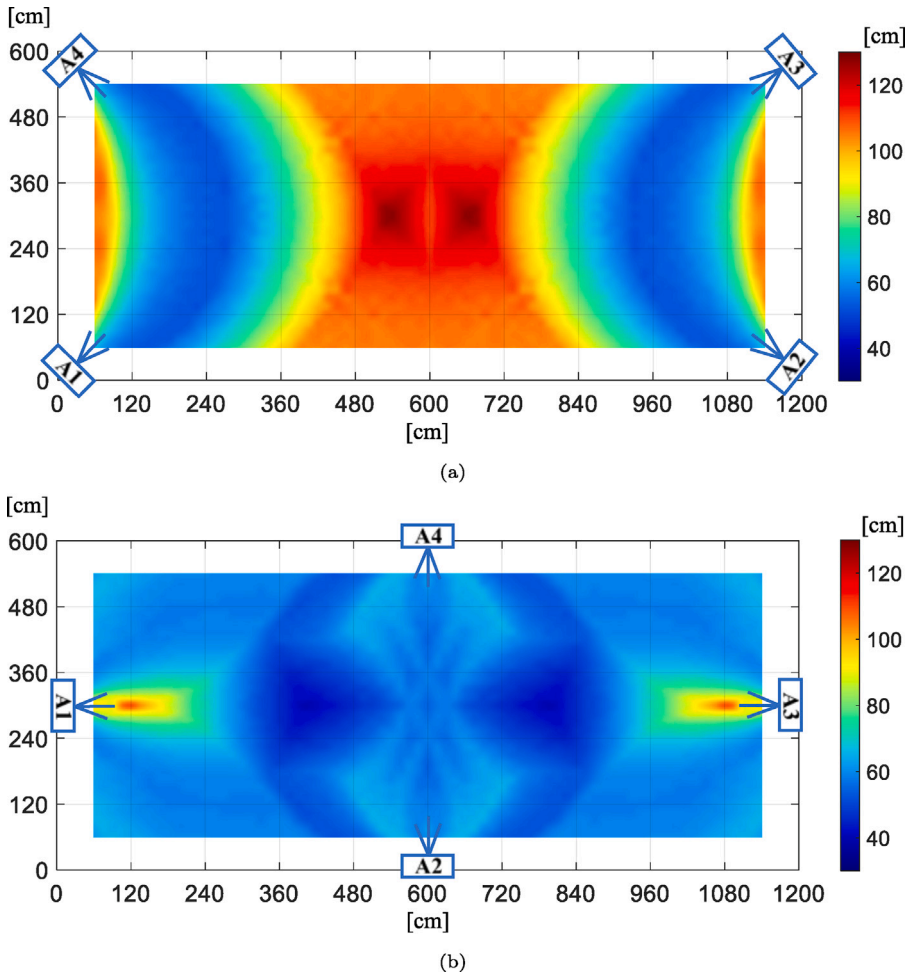

Fig. 10. Error heatmap in a setting with anchors placed in the corners (a) and in the middle of walls (b).

Fig. 11. Ublox anchor mounted on a graduated gimbal and tag.

5.3. Results

In this section, we present the outcomes achieved through the implementation of the proposed algorithms (see Section 4.2), culminating in an overview of the observed trend in azimuthal errors in our experiments. For each algorithm, we compute the 90th, 75th, and 50th percentiles of the localization error obtained as the Euclidean distance from the actual positions, namely the ground truth. Additionally, we utilize heatmaps to visualize the spatial distribution of these errors and employ Cumulative Distribution Functions (CDFs) to facilitate comparisons between the algorithms.

We compare the results of 5 algorithms:

- *Pure Barycenter*: a base-line algorithm that makes use of all the available intersection points;
- *No Outlier*: a base-line algorithm that eliminates the intersections that fall outside the room;
- *All-in Region*: the proposed algorithm reported in Section 4.2. We varied the azimuthal error impacting the size of the confidence regions, ranging from a minimum of 5° to a maximum of 15°, and the best results are obtained for an error equal to 13°.

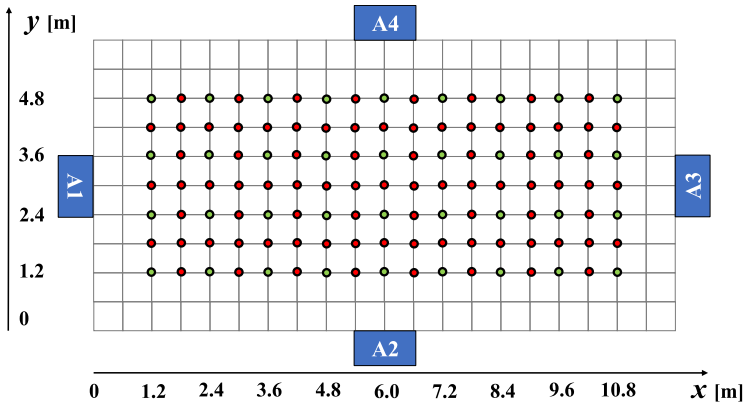

Fig. 12. Points used with the Calibration scenario (all points) and with the Static scenario (green points).

Table 2
Localization error for the 5 algorithms obtained with the Calibration dataset.

Algorithm	90th	75th	50th	Algorithm settings
Pure Barycenter	3.81	2.44	1.28	All intersections
NoOutlier	2.23	1.50	0.99	Only intersections inside room
All-in Region	1.97	1.43	0.90	Azimuth err. 13°, s = 1
All-in Circle	2.00	1.30	0.84	Radius 110 cm , s = 1
Cond. All-in Circle	**1.80**	**1.30**	**0.75**	Filtering far anchors (A1,A3)

Regarding the stop condition of the iteration process, we set the stop condition at a single intersection.

- *All-in Circle*: the proposed algorithm reported in Section 4.2. We varied the radius of the circle from 60 cm up to 2 m and the best results are obtained for a radius equal to 110 cm.
- *Conditional All-in Circle*: the proposed algorithm reported in Section 4.2. We filtered Anchor 1 and 3

Concerning the Calibration dataset, Table 2 reports the localization error's statistics (expressed in meters) for the five algorithms. Notably, the *Conditional All-in Circle* algorithm exhibits superior performance, with a 50th percentile localization error of 75 cm. In contrast, the *Pure Barycenter* algorithm yields a 50th percentile error of 1.28 m and a 90th percentile error of 3.81 m. Fig. 13 displays the localization error as an heatmap. For the shake of simplicity, we remove *All-in Region* due to its similarity to the *All-in Circle*.

To assess the performance further, we provide Cumulative Distribution Functions (CDFs) for the algorithms in Fig. 14. From the figure, it is possible to observe performance improvement of *Conditional All-in Circle* with respect to the three percentiles, 50th, 75th and 90th. Please note that the *Pure Barycenter* CDF has been excluded from the graph to avoid the necessity of applying a logarithmic scale.

We now assess the performance of the five algorithms using the Static dataset. In this case, the orientation of the target varies. It is worth noting that the orientation has a notable impact on the stability of Angle of Arrival (AoA) estimation in the azimuthal plane. In contrast to the Calibration dataset, where the estimated AoA remains relatively consistent, the Static dataset exhibits stability in only 60% of the samples, while the remaining 40% vary within a range of 5° to 15°. The worst results are observed when the target is oriented to the South (as shown in Table 3), while the best performance is achieved when the target faces North. Table 3 presents the performance of the five algorithms across four different orientations, while Fig. 15 provides a heatmap representation of localization errors. The heatmap is obtained by only comparing the performance between the least and most optimal algorithms. We also compute the CDF of the localization error by comparing the performance of the algorithms, as reported in Fig. 16. From the figure, we observe that also with the Static dataset,

Table 3
Localization error for the 5 algorithms obtained with the Static dataset.

Body orientation	Algorithm	90th	75th	50th
East	Pure Barycenter	5.76	2.32	1.09
	NoOutlier	2.09	1.58	0.94
	All-in Region	1.98	1.28	0.89
	All-in Circle	2.07	1.33	0.88
	Cond. All-inCircle	**1.87**	**1.31**	**0.88**
South	Pure Barycenter	5.64	3.29	1.88
	NoOutlier	2.61	2.18	1.73
	All-in Region	3.01	2.49	1.52
	All-in Circle	3.01	2.34	1.30
	Cond. All-in Circle	**2.30**	**1.79**	**1.23**
West	Pure Barycenter	4.56	2.56	1.69
	NoOutlier	2.24	1.73	1.29
	All-in Region	2.43	1.67	0.95
	All-in Circle	2.41	1.57	0.97
	Cond. All-in Circle	**1.75**	**1.27**	**0.92**
North	Pure Barycenter	4.70	2.24	1.50
	NoOutlier	2.46	1.73	1.15
	All-in Region	2.60	1.33	0.94
	All-in Circle	2.59	1.39	0.89
	Cond. All-in Circle	**1.80**	**1.12**	**0.74**

Conditional All-in Circle outperforms the other algorithms in all the orientations.

From the obtained results, it becomes evident that the *Pure Barycenter* algorithm, which utilizes all possible intersection points, performs the poorest. In contrast, the algorithm that removes intersections falling outside the room shows a significant error reduction when a straightforward filter is applied. Among the proposed algorithms, namely *All-in Region*, *All-in Circle* and *Conditional All-in Circle* they generally outperform *NoOutlier*. However, *All-in Region* comes at a higher computational cost and more complex implementation compared to the others. Its *All-in Circle* variant is lighter yet equally effective. The primary advantage of such algorithm is its ability to eliminate both inaccurately projected data outside the environment and internal data resulting from erroneous estimates due to environmental noise. Therefore, when defining the indoor environment's perimeter is challenging, *All-in Circle* represents the best choice. Nevertheless, it does not consistently improve every estimate over the *NoOutlier* algorithm. In simple terms, if the algorithm provides an accurate estimate based on the barycenter of two intersections outside its confidence region, it might still reject one of them, resulting in an increase in error rather than a decrease.

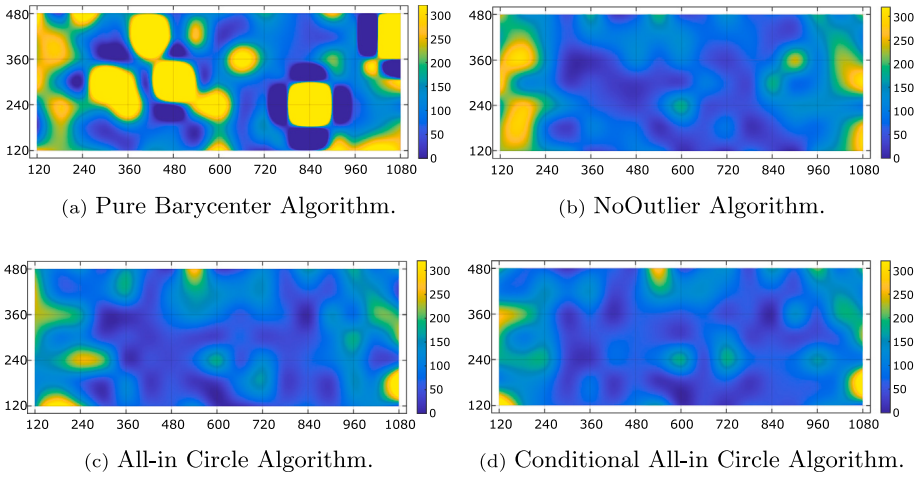

(a) Pure Barycenter Algorithm. (b) NoOutlier Algorithm.

(c) All-in Circle Algorithm. (d) Conditional All-in Circle Algorithm.

Fig. 13. Heatmap of the localization error obtained with the Calibration dataset.

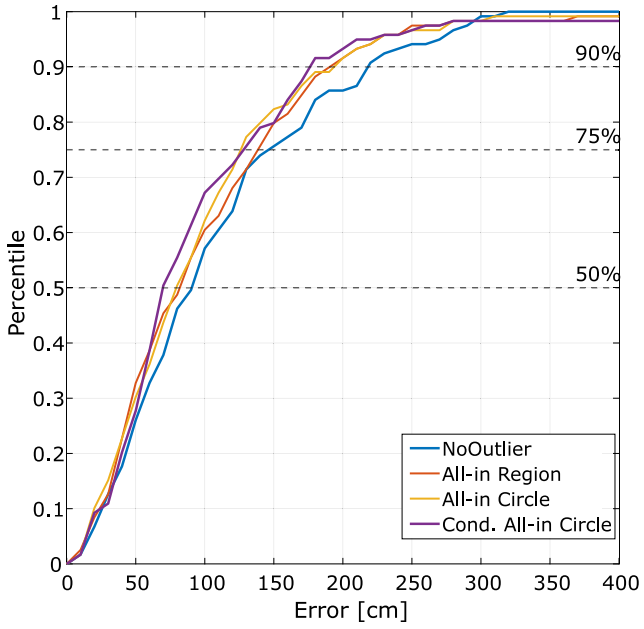

Fig. 14. CDF of the algorithms based on the Calibration dataset.

Table 4
Comparison with traditional methods.

Methods comparison					
Dataset		Method	Localization error [cm]		
			90th	75th	50th
Calibration dataset		LLS	194	138	94
		WLLS	198	**129**	77
		Cond. All-In	**180**	130	**75**
NLoS datasets	East	LLS	193	144	**71**
		WLLS	193	**128**	72
		Cond. All-In	**187**	131	88
	North	LLS	258	186	126
		WLLS	245	193	101
		Cond. All-In	**180**	**112**	**74**
	West	LLS	220	162	113
		WLLS	182	158	97
		Cond. All-In	**175**	**127**	**92**
	South	LLS	265	221	168
		WLLS	251	202	157
		Cond. All-In	**230**	**179**	**123**

The best outcomes were achieved with the last algorithm variant: *Conditional All-in Circle*. with this variant, the decision to use anchors is conditioned on their actual contribution to defining the confidence regions, based on the characteristics of the regions themselves. While, initially, we assumed a uniform distribution of a 5° error in estimating azimuthal angles, it is observed that the best settings for the algorithms' parameters ϵ and R are an average error of 13° for the azimuth and an equivalent radius of 110 cm.

Finally, we present the Table 4 that compares the percentile errors of the traditional LLS and WLLS algorithms with the proposed solution. Starting from the centroid calculated on all possible intersections of the directions yields a suboptimal solution compared to the LLS method, which serves as the lower limit to surpass. The optimal solution obtained with the WLLS method represents the upper bound, as it utilizes statistical information that our approach does not. The table shows encouraging results, as in all cases, the proposed method either matches or outperforms the LLS solution. In scenarios where the anchors were not always in line of sight, the algorithm provided even better results than the WLLS solution. Only in the EAST orientation did the median error fail to outperform the LLS method, but in this instance, the WLLS method also did not show any improvement.

6. Discussion

We now discuss two relevant issues that significantly affect the performance of the proposed algorithms. We study in Section 6.1 how the AoA's error varies with respect to the measurement angle. In Section 6.2 we discuss the theoretical limits of the proposed algorithms with a benchmark comparison.

6.1. Modeling the AoA's error

We now present the absolute errors in azimuthal angles obtained from our previous data collection campaign, as detailed in [13]. In this study, we start with the optimistic assumption that the average Angle of Arrival (AoA) error is set to 5°, as reported by the manufacturer's datasheet. However, it is important to note that the actual instrumental error may not be uniform, and environmental factors must also be considered. In Fig. 17, we illustrate the measured error along the sampling directions, which span from −76° to +76° for the anchor

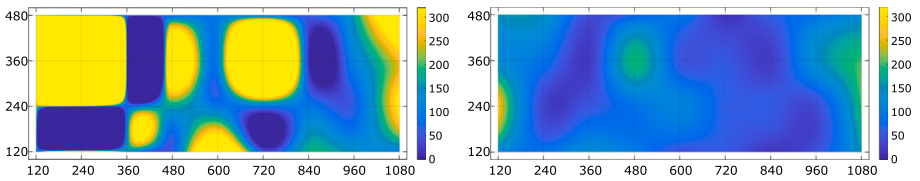

(a) Pure Barycenter Algorithm, East Orientation.

(b) Conditional All-in Circle Algorithm, East Orientation.

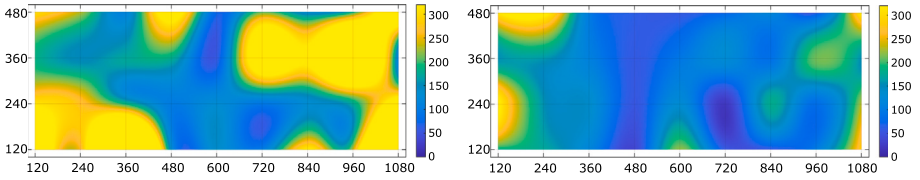

(c) Pure Barycenter Algorithm, South Orientation.

(d) Conditional All-in Circle Algorithm, South Orientation.

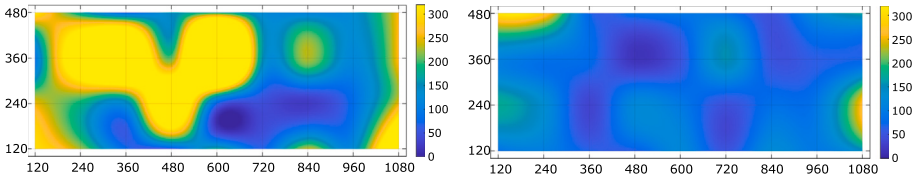

(e) Pure Barycenter Algorithm, West Orientation.

(f) Conditional All-in Circle Algorithm, West Orientation.

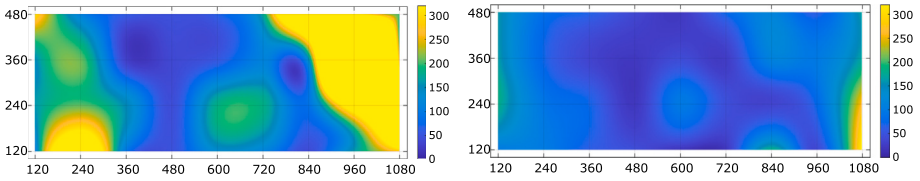

(g) Pure Barycenter Algorithm, North Orientation.

(h) Conditional All-in Circle Algorithm, North Orientation.

Fig. 15. Heatmap of the localization error obtained with the Static dataset comparing best and worst algorithm.

positioned on the longer side of the room. Data points are interpolated using a ninth-degree polynomial (blue plot), revealing that the error varies depending on the observation angle of the target. Within a field of view of 90° (FoV-90), that is an angular range from −45° to +45°, the azimuth error remains below 10°. However, once this range is exceeded, the AoA error increases to as much as 40°.

To elucidate the limits of assuming a uniform AoA error, we present in Fig. 18 the CDFs of the theoretical localization error. This error is determined by calculating, at each point, the width of the Confidence Regions. The regions are generated under the assumption of a uniform average error of 5°, 10°, 15°. In the figure the CDFs are compared with the *NoOutLier* and *Conditional All-in Circle* algorithms in addition to a third a posteriori algorithm called *Best Combination* that will be introduced in the next section. The plotting is obtained from the Calibration dataset. From the figure, we observe that up to the 75th percentile *Cond.All-in Circle* behaves like the CDF based on an angular error of 10° (purple plots) while *NoOutLier* is closer to the CDF with an angular error of 15° (light blue plots). Finally, the CDF based on angular error of 5° is comparable to the *Best Combination* algorithm (black-dashed line).

6.2. Theoretical limits of the proposed algorithms

Despite the performance improvements obtained with the proposed algorithms, several issues remain unanswered. In particular, three research questions still require further investigation: What is the optimal number of anchor's intersections to consider during the algorithm's recursion? Furthermore, how can we measure the actual improvement achieved by these algorithms compared to the straightforward yet effective *NoOutlier* algorithm? Moreover, is it possible to enhance the algorithm further, perhaps by performing additional selection among various intersections?

To address the aforementioned questions, we evaluated the performance of an ideal 'a posteriori' algorithm. The adopted approach assumes the full knowledge of the target's ground truth (the actual location for every measurement point) and it determines the best the combination of intersections whose barycenter minimizes the error. This approach involves calculating all possible combinations of intersections and their barycenters, allowing us to assess the quality of the measurements made and the effectiveness of the proposed algorithms.

The number of potential barycenters equals the sum of simple combinations of s intersections, equivalent to the number of partitions of a set with s elements, minus the empty set:

$$\sum_{k=1}^{s} \binom{s}{k} = 2^s - 1;$$

with $s = 6$ intersections, we have 63 distinct combinations. As result, for each of the 119 positions in the Calibration dataset, we calculated 63 barycenters, computed the Euclidean error relative to the ground truth, and organized the results. By selecting the minimum error across all positions, we can establish, given a measurement, the lower bound

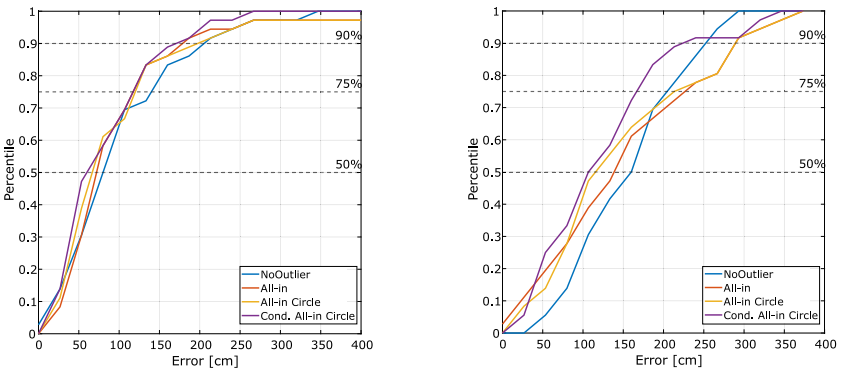

(a) East Orientation. (b) South Orientation.

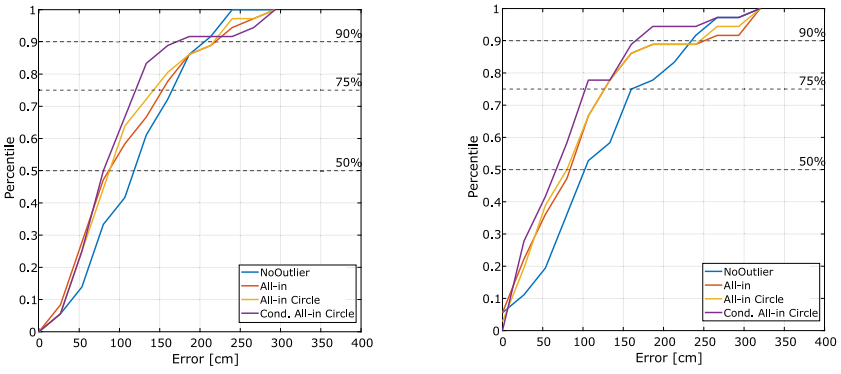

(c) West Orientation. (d) North Orientation.

Fig. 16. CDF of best/worst algorithms based on the Static dataset.

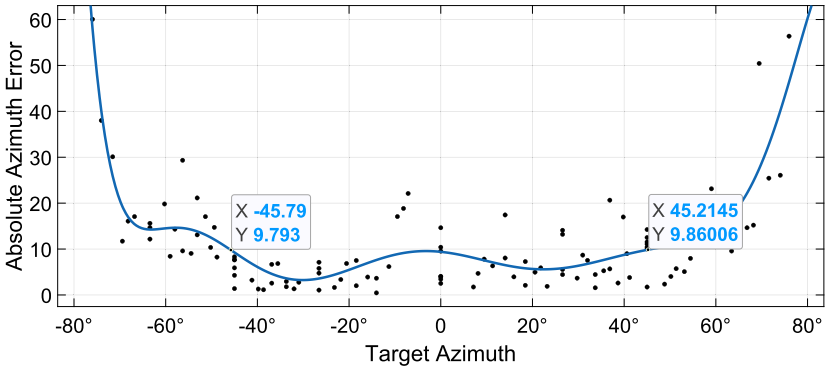

Fig. 17. Analysis of the azimuth angle.

of any algorithm, as depicted in Fig. 18 with the CDF *Best Combination*. Additionally, by sorting the errors in descending order, for each position, we determined the 10th, 25th and 50th percentile of the errors, thus creating a performance scale for the algorithms.

The scale of such ideal algorithms is illustrated in Fig. 19. The dotted plots represents the best performance on the left to the median one on the right side. The figure also shows the CDFs of the *NoOutlier* and *Conditional All-in Circle* algorithms. The first one aligns with the median error CDF (solid and dotted light blue plots), while the proposed algorithm aligns with the 25th percentile (solid and dotted purple plots). Thus, we can say that the improvement of *Conditional All-in Circle* with respect *NoOutlier* is about a quartile.

Back to Fig. 19, it is worth noting that *Best Combination* CDF, up to the 75th percentile, resembles the theoretical CDF for azimuthal errors of 5°. This suggests that a certain number of measurements with errors below 5° were indeed recorded. However, these measurements constitute only a percentage, and as observed previously, errors increase rapidly outside an angular range of 90°.

The post-evaluation curves also provides valuable insights into the number of intersections used to compute the barycenters. Table 5 illustrates for each curve the percentage of barycenters calculated using a single intersection, all the way up to the maximum of 6 intersections.

It is noticeable that the curve representing the lower bound of the performance has the highest percentage of barycenters derived from a single intersection. As performance deteriorates, the utilization of barycenters formed by multiple intersections increases. Consequently, it is reasonable to iterate the All-in algorithms until reaching the termination condition of only one intersection. However, it is important to note that the algorithm does not necessarily converge to the optimal solution among the six available intersections. This is precisely why the exclusion of intersections generated by anchors located too far away

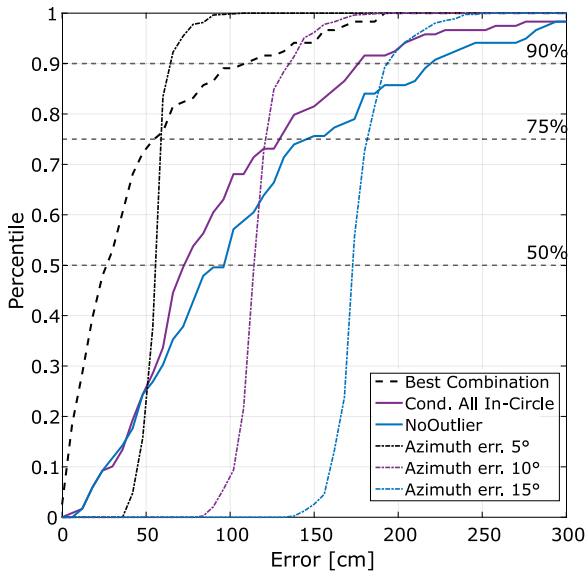

Fig. 18. Performance comparison of a uniform AoA error (5°, 10°, 15°) with respect to real-world measurements.

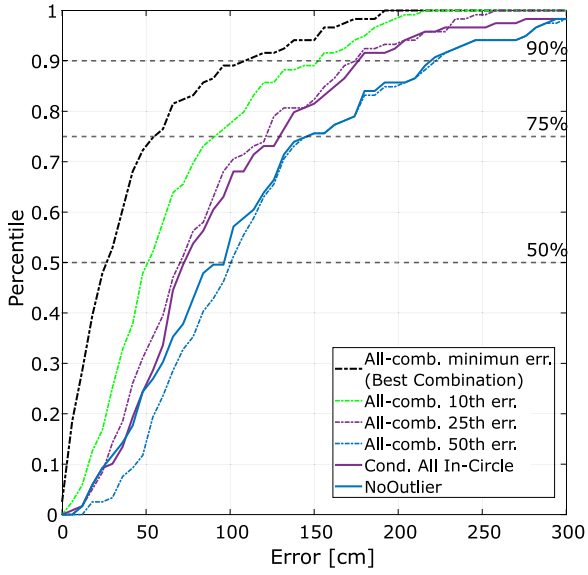

Fig. 19. Comparing the performance scale: from the lower bound to the proposed algorithms.

Table 5
Percentages of the number of intersections used in a posteriori position estimation.

A posteriori	Number of intersections					
Algs	1	2	3	4	5	6
Best Combination	46%	32%	16%	3%	3%	0%
10th Best Comb.	13%	36%	36%	14%	0%	0%
25th Best Comb.	9%	22%	25%	28%	13%	3%
50th Best Comb.	9%	15%	23%	22%	19%	12%

reduces the likelihood of selecting a suboptimal combination and yields improved results.

Finally, Table 6 presents an outlook of the problem's magnitude. As the number of anchors varies, intersections increase following the sequence of triangular numbers, i.e. $O(n^2)$, while the number of possible combinations grows at more than an exponential rate. It will be interesting to assess how the distribution of combinations in Table 5 changes with the increase in the number of anchors/intersections.

Table 6
Problem size as the number of anchors varies.

Problem size							
#Anchors $O(n)$	2	3	**4**	5	6	7	8
#Intersections $O(n^2)$	1	3	**6**	10	15	21	28
#Combinations $O(2^{(n^2)})$	1	7	**63**	1023	32.767	2.097.151	268.435.455

7. Conclusions

Localizing users within indoor environments represents a fundamental component of intelligent environments. This capability is crucial for comprehending user contexts and adapting to changes in the surrounding environment. Under this respect, several techniques can be adopt to estimate the user's position, ranging from RSS, AoA and ToF. In this work, we focus on the use of Angle of Arrival to design and evaluate a set of algorithms for indoor localization. We discuss the limitations of the traditional triangulation-based approach and introduce a novel method guided by the uncertainty of the measurements, namely the Confidence Region. Additionally, we propose optimized version of the algorithms with reduced computational costs. We compare the performance of the proposed algorithms with an experimental dataset [13] collected at realistic conditions. From our results, it is evident the performance improvement of those algorithms leveraging confidence region concept and to this end, we have also identified an effective method for comparing and evaluating the performance of algorithms through a posteriori combinatorial analysis. Furthermore, we also present a simulation tool useful to determine the optimal anchors' layout. Having a simulator that provides insights into both the placement of anchors and their impact on position estimation is pivotal for any study.

Our goal is to explore the potential of the Direction Finding specification to develop indoor localization algorithms and test their performance in real-world settings. Our results reveal three key findings: (1) The angle of arrival error varies significantly with the measurement angle. Specifically, beyond the FoV-90, accuracy decreases at peripheral angles between the tag and the antenna, which negatively impacts the performance of the algorithms. (2) The estimation of target locations based on confidence regions has proven effective. We found that anchors that do not contribute to reducing uncertainty should be excluded from the estimation process, as they may negatively impact the accuracy of the target's location, and (3) The algorithm is effective, even when starting from a suboptimal solution that considers all possible direction intersections, and remains robust when the tag's orientation is modified, maintaining line of sight with only one anchor at a time.

Based on these findings, we believe that AoA techniques provided by the Direction Finding specification are a viable technology for indoor settings. The results we have obtained indicate significant potential for enhancing localization accuracy. Following this consideration, we foresee several future research directions.

Firstly, the proposed algorithms can be compared with clustering algorithms such as K-Means and DBSCAN, which, although designed for large datasets, can select a cluster of closest intersections. Additionally, machine learning techniques based on neural networks should be tested to identify patterns in the distribution of combinations presented in Table 5. This could be further enhanced by incorporating the elevation angle information, which was excluded in this study. Secondly, it is important to consider the disruptions present in real indoor environments. As the number of targets increases, signal packet losses and noise are likely to increase, opening to possible scalability challenges. We also plan to expand the dataset we published with a new data collection campaign based on anchors equipped with 8-element URA (Uniform

Distributed Array) antennas. Such anchors are designed to improve the accuracy of AoA estimation also when the tag is positioned on peripheral areas with respect to the anchor. Our goal is deploying an extended infrastructure of anchors covering a wide indoor area for a variety of tests in a daily working environment characterized by multiple target's users. One final consideration is the possibility of integrating BT5.1 Direction Finding technology with smart devices. While this technology is expected to improve soon, there are limitations regarding the size of the antenna array. These limitations may reduce the feasibility of deploying multiple antennas on a smart device. Therefore, we find it ideal to use BT5.1 with a permanent infrastructure, featuring anchors deployed in strategic locations.

Characterizing complex electromagnetic environments is a challenging task due to the variability introduced by several factors, such as interference from multiple sources of electromagnetic radiation, the presence of obstacles, and the reflection and attenuation of signals. While obstacles caused by fixed furniture can be managed through sensor network calibration techniques to improve performance, those caused by the presence of people are much more difficult to handle. In our experiments, the tag worn by a single person was consistently in line of sight with only one of the four installed anchors at a time. Under these conditions, the percentage of errors in angle estimation doubled compared to the calibration scenario, where all anchors were always in sight. In the scenarios considered, it was observed that optimal methods based on statistical data can become inefficient and are often outperformed by techniques that aim to exclude outliers. Further investigation is required to evaluate the effects in crowded environments. In the current scenario, the body of a single person attenuates the signal toward anchors that are not in line of sight and enhances the reception of reflected signals with greater power. In a crowded environment, all signals may be equally attenuated, making techniques based on the angle of arrival potentially more effective than those relying on signal strength.

In real-world, densely populated scenarios, such as museums, we believe that addressing all possible disturbances may require the integration of these devices with complementary sensors to mitigate the inaccuracies of RF-based techniques. More generally, we consider it crucial to combine heterogeneous sensing information, such as inertial sensors, using filtering mechanisms like Particle filtering. In previous scenarios, inertial sensors play a crucial role in preserving the target's direction. Their simultaneous adoption could potentially enhance the performance of an indoor localization system with moving targets, thus mitigating the limitations of relying solely on a single technology.

CRediT authorship contribution statement

Francesco Furfari: Writing – original draft, Methodology, Investigation, Formal analysis, Conceptualization. **Michele Girolami:** Writing – review & editing, Writing – original draft, Methodology, Investigation, Conceptualization. **Fabio Mavilia:** Writing – original draft, Methodology, Investigation, Formal analysis, Conceptualization. **Paolo Barsocchi:** Writing – review & editing, Writing – original draft, Supervision, Conceptualization.

Declaration of competing interest

The authors declare that they have no known competing financial interests or personal relationships that could have appeared to influence the work reported in this paper.

Acknowledgments

This work is partially supported by the ChAALenge project CUP: B89J22002310005 and co-funded by European Union - Next Generation EU, in the context of The National Recovery and Resilience Plan, Investment Partenariato Esteso PE8 "Conseguenze e sfide dell'invecchiamento", Project Age-IT (PNRR), CUP: B83C22004800006.

Table A.7
List of all the abbreviations used in the paper.

Abbreviation	Definition
AoA	Angle of Arrival
AoD	Angle of Departure
CDF	Cumulative Distribution Function
CIR	Carrier-to-Interference Ratio
CR	Confidence Region
CSI	Channel State Information
CTE	Constant Tone Extension
DBSCAN	Density-Based Spatial Clustering of Applications with Noise
DF	Direction Finding
DFL	Device-Free Localization
ESPRIT	Estimation of Signal Parameters via Rotational Invariance Techniques
FoV	Field of View
GDOP	Geometric Dilution of Precision
HDOP	Horizontal Dilution of Precision
IoT	Internet of Things
IPLE	Improved Pseudo-Linear Estimator
IQ	In-Phase and Quadrature
IWIV	Improved Weighted Instrumental Variable Estimator
LLS	Linear Least-Squares
LoS	Line of Sight
MPR	Modified Polar Representation
MUSIC	Multiple Signal Classification
NLoS	Non line of Sight
PDoA	Phase Difference of Arrival
PDU	Protocol Data Unit
RF	Radio-Frequency
RSS	Received Signal Strength
RSSI	Received Signal Strength Indicator
SDR	Software Defined Radio
ToF	Time of Flight
ULA	Uniform Linear Array
URA	Uniform Rectangular Array
UWB	Ultra Wide Band
WLLS	Weighted Linear Least-Squares
WLS	Weighted Least-Squares
WLS-BR	Weighted Least-Squares Bias-Reduced

Appendix. Abbreviations

In this section, we report Table A.7 which lists all the abbreviations used in the paper.

Data availability

The dataset is available to the research community.

References

[1] C. Laoudias, A. Moreira, S. Kim, S. Lee, L. Wirola, C. Fischione, A survey of enabling technologies for network localization, tracking, and navigation, IEEE Commun. Surv. Tutor. 20 (4) (2018) 3607–3644, http://dx.doi.org/10.1109/COMST.2018.2855063.

[2] S. Hayward, K. van Lopik, C. Hinde, A. West, A survey of indoor location technologies, techniques and applications in industry, Internet Things 20 (2022) 100608, http://dx.doi.org/10.1016/j.iot.2022.100608, URL https://www.sciencedirect.com/science/article/pii/S2542660522000907.

[3] F. Potortì, A. Crivello, F. Palumbo, M. Girolami, P. Barsocchi, Trends in smartphone-based indoor localisation, in: 2021 International Conference on Indoor Positioning and Indoor Navigation, IPIN, IEEE, 2021, pp. 1–7.

[4] Q. Spencer, B. Jeffs, M. Jensen, A. Swindlehurst, Modeling the statistical time and angle of arrival characteristics of an indoor multipath channel, IEEE J. Sel. Areas Commun. 18 (3) (2000) 347–360, http://dx.doi.org/10.1109/49.840194.

[5] R. Faragher, R. Harle, Location fingerprinting with bluetooth low energy beacons, IEEE J. Sel. Areas Commun. 33 (11) (2015) 2418–2428, http://dx.doi.org/10.1109/JSAC.2015.2430281.

[6] M. Collotta, G. Pau, A novel energy management approach for smart homes using bluetooth low energy, IEEE J. Sel. Areas Commun. 33 (12) (2015) 2988–2996, http://dx.doi.org/10.1109/JSAC.2015.2481203.

[7] Bluetooth Special Interest Group (SIG). Bluetooth 5.1 Direction Finding, Tech. Rep., 2019, URL https://www.bluetooth.com/wp-content/uploads/2019/05/BTAsia/1145-NORDIC-Bluetooth-Asia-2019Bluetooth-5.1-Direction-Finding-Theory-and-Practice-v0.pdf.

[8] F. Furfari, P. Barsocchi, M. Girolami, F. Mavilia, Modelling the localization error of an AoA-based localization system, in: 2023 19th International Conference on Intelligent Environments, IE, 2023, pp. 1–4, http://dx.doi.org/10.1109/IE57519.2023.10179094.

[9] F. Mavilia, P. Barsocchi, F. Furfari, M. Girolami, Evaluating the impact of anchors deployment for an AoA-based indoor localization system, in: 2023 18th Wireless on-Demand Network Systems and Services Conference, WONS, 2023, pp. 20–23, http://dx.doi.org/10.23919/WONS57325.2023.10061949.

[10] G. Pau, F. Arena, Y.E. Gebremariam, I. You, Bluetooth 5.1: an analysis of direction finding capability for high-precision location services, Sensors 21 (11) (2021) http://dx.doi.org/10.3390/s21113589.

[11] A.M.L. Peter J. Rousseeuw, Robust Regression and Outlier Detection, John Wiley & Sons, Inc., 1987.

[12] P.J. Rousseeuw, M. Hubert, Anomaly detection by robust statistics, WIREs Data Min. Knowl. Discov. 8 (2) (2018) e1236, http://dx.doi.org/10.1002/widm.1236.

[13] M. Girolami, F. Furfari, P. Barsocchi, F. Mavilia, A bluetooth 5.1 dataset based on angle of arrival and RSS for indoor localization, IEEE Access 11 (2023) 81763–81776, http://dx.doi.org/10.1109/ACCESS.2023.3301126.

[14] B. Yang, L. Guo, R. Guo, M. Zhao, T. Zhao, A novel trilateration algorithm for RSSI-based indoor localization, IEEE Sens. J. 20 (14) (2020) 8164–8172, http://dx.doi.org/10.1109/JSEN.2020.2980966.

[15] M. Girolami, P. Barsocchi, F. Furfari, D. La Rosa, F. Mavilia, Evaluation of angle of arrival in indoor environments with bluetooth 5.1 direction finding, in: 2022 18th International Conference on Wireless and Mobile Computing, Networking and Communications, WiMob, 2022, pp. 284–289, http://dx.doi.org/10.1109/WiMob55322.2022.9941619.

[16] J. Niu, B. Wang, L. Shu, T.Q. Duong, Y. Chen, ZIL: an energy-efficient indoor localization system using ZigBee radio to detect WiFi fingerprints, IEEE J. Sel. Areas Commun. 33 (7) (2015) 1431–1442, http://dx.doi.org/10.1109/JSAC.2015.2430171.

[17] F. Furfari, A. Crivello, P. Baronti, P. Barsocchi, M. Girolami, F. Palumbo, D. Quezada-Gaibor, G.M. Mendoza Silva, J. Torres-Sospedra, Discovering location based services: A unified approach for heterogeneous indoor localization systems, Internet Things 13 (2021) 100334, http://dx.doi.org/10.1016/j.iot.2020.100334, URL https://www.sciencedirect.com/science/article/pii/S2542660520301657.

[18] F. Potortì, A. Crivello, M. Girolami, P. Barsocchi, E. Traficante, Localising crowds through Wi-Fi probes, Ad Hoc Netw. 75–76 (2018) 87–97, http://dx.doi.org/10.1016/j.adhoc.2018.03.011, URL https://www.sciencedirect.com/science/article/pii/S1570870518300696.

[19] Y. He, A. Behnad, X. Wang, Accuracy analysis of the two-reference-node angle-of-arrival localization system, IEEE Wirel. Commun. Lett. 4 (3) (2015) 329–332, http://dx.doi.org/10.1109/LWC.2015.2415788.

[20] L. Badriasl, K. Dogancay, Three-dimensional target motion analysis using azimuth/elevation angles, IEEE Trans. Aerosp. Electron. Syst. 50 (4) (2014) 3178–3194, http://dx.doi.org/10.1109/TAES.2014.120251.

[21] Y. Wang, K.C. Ho, An asymptotically efficient estimator in closed-form for 3-D AOA localization using a sensor network, IEEE Trans. Wireless Commun. 14 (12) (2015) 6524–6535, http://dx.doi.org/10.1109/TWC.2015.2456057.

[22] Y. Zou, L. Wu, J. Fan, H. Liu, A convergent iteration method for 3-D AOA localization, IEEE Trans. Veh. Technol. 72 (6) (2023) 8267–8271, http://dx.doi.org/10.1109/TVT.2023.3242054.

[23] Y. Sun, K.C. Ho, Q. Wan, Eigenspace solution for AOA localization in modified polar representation, IEEE Trans. Signal Process. 68 (2020) 2256–2271, http://dx.doi.org/10.1109/TSP.2020.2981773.

[24] G. Wang, P. Xiang, K.C. Ho, Bias reduced semidefinite relaxation method for 3-D moving object localization using AOA, IEEE Trans. Wireless Commun. (2023) 1, http://dx.doi.org/10.1109/TWC.2023.3250420.

[25] M. Cominelli, P. Patras, F. Gringoli, Dead on arrival: an empirical study of the bluetooth 5.1 positioning system, in: Proceedings of the 13th International Workshop on Wireless Network Testbeds, Experimental Evaluation and Characterization, WiNTECH '19, Association for Computing Machinery, New York, NY, USA, 2019, pp. 13–20, http://dx.doi.org/10.1145/3349623.3355475.

[26] P. Sambu, M. Won, An experimental study on direction finding of bluetooth 5.1: indoor vs outdoor, in: IEEE Wireless Communications and Networking Conference, 2022, pp. 1934–1939, http://dx.doi.org/10.1109/WCNC51071.2022.9771930.

[27] G. Pan, J. Ho, Indoor positioning experiments based on BT 5.1, in: 2022 IEEE 4th International Conference on Power, Intelligent Computing and Systems, ICPICS, IEEE, 2022, pp. 687–692.

[28] H. Ye, B. Yang, Z. Long, C. Dai, A method of indoor positioning by signal fitting and PDDA algorithm using BLE AOA device, IEEE Sens. J. 22 (8) (2022) 7877–7887.

[29] Y. Zheng, M. Sheng, J. Liu, J. Li, Exploiting AoA estimation accuracy for indoor localization: a weighted aoa-based approach, IEEE Wirel. Commun. Lett. 8 (1) (2019) 65–68, http://dx.doi.org/10.1109/LWC.2018.2853745.

[30] Y. Fu, P. Chen, S. Yang, J. Tang, An indoor localization algorithm based on continuous feature scaling and outlier deleting, IEEE Internet Things J. 5 (2) (2018) 1108–1115, http://dx.doi.org/10.1109/JIOT.2018.2795615.

[31] G. Boquet, A. Boquet-Pujadas, I. Pisa, A. Dabak, X. Vilajosana, B. Martinez, Indoor position estimation using angle of arrival measurements: An efficient multi-anchor approach with outlier rejection, Internet Things 26 (2024) 101236, http://dx.doi.org/10.1016/j.iot.2024.101236, URL https://www.sciencedirect.com/science/article/pii/S254266052400177X.

[32] S. Yang, D. Zhang, R. Song, P. Yin, Y. Chen, Multiple WiFi access points co-localization through joint AoA estimation, IEEE Trans. Mob. Comput. 23 (2) (2024) 1488–1502, http://dx.doi.org/10.1109/TMC.2023.3239377.

[33] A.H. Chughtai, M. Tahir, M. Uppal, Outlier-robust filtering for nonlinear systems with selective observations rejection, IEEE Sens. J. 22 (7) (2022) 6887–6897, http://dx.doi.org/10.1109/JSEN.2022.3152609.

[34] L. Yang, N. Wu, B. Li, W. Yuan, L. Hanzo, Indoor localization based on factor graphs: a unified framework, IEEE Internet Things J. 10 (5) (2023) 4353–4366, http://dx.doi.org/10.1109/JIOT.2022.3215714.

[35] G. Guo, R. Chen, X. Niu, K. Yan, S. Xu, L. Chen, Factor graph framework for smartphone indoor localization: integrating data-driven PDR and Wi-Fi RTT/RSS ranging, IEEE Sens. J. 23 (11) (2023) 12346–12354, http://dx.doi.org/10.1109/JSEN.2023.3267121.

[36] F. Potortì, S. Park, et al., The IPIN 2019 indoor localisation competition—Description and results, IEEE Access 8 (2020) 206674–206718, http://dx.doi.org/10.1109/ACCESS.2020.3037221.

[37] F. Potortì, J. Torres-Sospedra, et al., Off-line evaluation of indoor positioning systems in different scenarios: the experiences from IPIN 2020 competition, IEEE Sens. J. 22 (6) (2022) 5011–5054, http://dx.doi.org/10.1109/JSEN.2021.3083149.

[38] K. Weiler, P. Atherton, Hidden surface removal using polygon area sorting, ACM SIGGRAPH Comput. Graph. 11 (2) (1977) 214–222.

[39] I. Sharp, K. Yu, Y.J. Guo, GDOP analysis for positioning system design, IEEE Trans. Veh. Technol. 58 (7) (2009) 3371–3382, http://dx.doi.org/10.1109/TVT.2009.2017270.

Francesco Furfari received the Ph.D. degree in information engineering from the University of Pisa, Pisa, Italy, in 2009. He is currently a Researcher with the Information Science and Technologies Institute (ISTI), National Research Council (CNR), Pisa, Italy. He coordinated several European projects on Ambient Assisted Living for ISTI-CNR, and is the Creator of the EvAAL international competition. His research interests include wireless sensor networks, mobile middleware, IoT, and indoor localization.

Michele Girolami received the M.Sc. and Ph.D. degrees in computer science from the University of Pisa, Pisa, Italy, in 2007 and 2015, respectively. He is currently with ISTICNR as a Researcher with the Wireless Network Laboratory. He participates to several EU projects and as national research projects. His research interests are mainly focused on indoor localization, proximity detection, pervasive computing and Internet of Things. He also supports the organization of the IPIN competition and he has been serving with several roles for the organization of workshops and international conferences.

Fabio Mavilia received the Graduate degree in electronic engineering from the University of Pisa, Pisa, Italy, in 2012. As a member of the Wireless Network Laboratory, he currently holds the position of Researcher with the Institute of Information Science and Technologies National Research Council of Italy. His research interests include Internet of Things and Cyber–Physical Systems, with a particular focus on Ambient Intelligence. In particular, his work is focused on development of embedded platforms for wireless sensor networks and of algorithms for indoor activity recognition and for indoor localization, by using unobtrusive sensing devices based on radio frequency technologies.

Paolo Barsocchi received the M.Sc. and Ph.D. degrees in information engineering from the University of Pisa, Pisa, Italy, in 2003 and 2007, respectively. He is currently a Researcher with the Information Science and Technologies Institute, National Research Council, Pisa, Italy. He has coauthored more than 100 articles published in international journals and conference proceedings. His research interests are mainly focused in the areas of the IoT, cyber–physical systems, indoor localization, and radio channel signal processing. He is also a member of numerous program committees and Editorial Board of international journals, and the Program Chair and the Co-Chair of several conferences.